Ground-state phases of a mixture of spin-1 and spin-2 Bose-Einstein condensates

Naoki Irikura,[1] Yujiro Eto,[2] Takuya Hirano,[3] and Hiroki Saito[1]
[1]*Department of Engineering Science, University of Electro-Communications, Tokyo 182-8585, Japan*
[2]*National Institute of Advanced Industrial Science and Technology (AIST), NMIJ, Tsukuba, Ibaraki 305-8568, Japan*
[3]*Department of Physics, Gakushuin University, Tokyo 171-8588, Japan*

(Received 14 December 2017; published 13 February 2018)

We investigate the ground-state phases of a mixture of spin-1 and spin-2 Bose-Einstein condensates at zero magnetic field. In addition to the intraspin interactions, two spin-dependent interaction coefficients are introduced to describe the interspin interaction. We systematically explore the wide parameter space, and obtain phase diagrams containing a rich variety of phases. For example, there exists a phase in which the spin-1 and spin-2 vectors are tilted relative to each other breaking the axial symmetry.

DOI: 10.1103/PhysRevA.97.023622

I. INTRODUCTION

There is a wide variety of quantum fluids with internal degrees of freedom, such as superfluid ^{3}He [1], p-wave and d-wave superconductors [2], possible superfluids in neutron stars [3,4], and spinor Bose-Einstein condensates (BECs) of atomic gases [5,6]. In these systems, the order parameters have spin or angular momentum degrees of freedom, and their ground-state phases, dynamics, and topological excitations are richer than those of single-component superfluids. If two or more quantum fluids with internal degrees of freedom are mixed, the order-parameter space is greatly extended and the physics is further enriched.

Spinor BECs of ultracold atoms are suitable systems for realizing such a mixture of quantum fluids due to their high controllability. However, in most previous experiments, spinor BECs of spin-1, spin-2, and spin-3 atoms have been realized only individually [7–11]. The ground state of a spin-1 BEC can be ferromagnetic or antiferromagnetic, and topological excitations, such as monopoles [12], skyrmions [13], half-quantum vortices [14], and knots [15], are possible. A spin-2 BEC is more intriguing because of the presence of the cyclic phase and non-Abelian vortices [16–18]. We expect that a mixture of such spinor BECs will exhibit novel quantum phases and topological excitations. A mixture of spin-1 and spin-1 BECs has been studied theoretically and phase diagrams and many-body properties have been determined [19–29]. The spin dynamics in a mixture of a spin-1 ^{23}Na BEC and a spin-1 ^{87}Rb thermal gas have been observed experimentally [30].

Recently, a mixture of spin-1 and spin-2 ^{87}Rb BECs was realized experimentally, and the spin dynamics were observed [31]. Motivated by this experiment, in the present paper we theoretically investigate the ground-state phase diagrams of the mixture of spin-1 and spin-2 BECs at zero magnetic field. The spin-1 and spin-2 BECs have one and two spin-dependent interaction coefficients, respectively. In addition to these intraspin interactions, in a spinor mixture we must consider the interspin interaction, which is described by two spin-dependent interaction coefficients for the spin-1 and spin-2 mixture. This gives a total of five spin-dependent interaction coefficients. We therefore study the ground-state phase diagrams by varying these five interaction coefficients. Using the Monte Carlo method, we determine the phase diagrams for various sets of the parameters. Unlike for the phase diagrams of the individual spin-1 and spin-2 BECs, the spinor mixture has phases that continuously change with respect to the interaction coefficients, including phases in which the spin-1 and spin-2 vectors are tilted from each other, breaking the axial symmetry. According to the interaction coefficients measured in Ref. [31], the ground state of the mixture of spin-1 and spin-2 ^{87}Rb BECs is different from that of the individual spin-1 and spin-2 BECs.

This paper is organized as follows. Section II presents the problem and reviews the ground states of spin-1 and spin-2 BECs. Section III details the numerical calculations and the various phase diagrams of the spinor mixture. Section IV provides the conclusions of this study.

II. FORMULATION OF THE PROBLEM

The spin state of spin-1 and spin-2 atoms are denoted by $|f,m\rangle$, where $f = 1,2$ and $m = -f, -f+1, \ldots, f$. We consider BECs with spin-1 and spin-2 atoms at zero temperature and zero magnetic field in the mean-field approximation. The macroscopic wave function for the BEC of spin state $|f,m\rangle$ is expressed as $\psi_m^{(f)}(\boldsymbol{r}) = \sqrt{\rho_f(\boldsymbol{r})}\zeta_m^{(f)}(\boldsymbol{r})$, where $\rho_f(\boldsymbol{r})$ is the density and $\zeta_m^{(f)}(\boldsymbol{r})$ is the complex spin vector normalized as $\sum_m |\zeta_m^{(f)}(\boldsymbol{r})|^2 = 1$. The energy E_f of a spin-f BEC with atomic mass M_f confined in a trap potential $V_f(\boldsymbol{r})$ is given by [5,6,16,17]

$$E_1 = \int d\boldsymbol{r} \sum_{m=-1}^{1} \psi_m^{(1)*}(\boldsymbol{r})\left[-\frac{\hbar^2}{2M_1}\nabla^2 + V_1(\boldsymbol{r})\right]\psi_m^{(1)}(\boldsymbol{r}) + \frac{1}{2}\int d\boldsymbol{r}\left[g_0^{(1)} + g_1^{(1)}\boldsymbol{F}^{(1)}(\boldsymbol{r})\cdot\boldsymbol{F}^{(1)}(\boldsymbol{r})\right]\rho_1^2(\boldsymbol{r}) \quad (1)$$

for a spin-1 BEC and

$$E_2 = \int d\boldsymbol{r} \sum_{m=-2}^{2} \psi_m^{(2)*}(\boldsymbol{r}) \Big[-\frac{\hbar^2}{2M_2}\nabla^2 + V_2(\boldsymbol{r}) \Big] \psi_m^{(2)}(\boldsymbol{r}) + \frac{1}{2}\int d\boldsymbol{r} \big[g_0^{(2)} + g_1^{(2)} \boldsymbol{F}^{(2)}(\boldsymbol{r}) \cdot \boldsymbol{F}^{(2)}(\boldsymbol{r}) + g_2^{(2)} \big| A_0^{(2)}(\boldsymbol{r}) \big|^2 \big] \rho_2^2(\boldsymbol{r}) \tag{2}$$

for a spin-2 BEC, where

$$\boldsymbol{F}^{(f)}(\boldsymbol{r}) = \sum_{mm'} \zeta_m^{(f)*}(\boldsymbol{r}) \boldsymbol{S}_{mm'}^{(f)} \zeta_{m'}^{(f)}(\boldsymbol{r}) \tag{3}$$

is the mean spin vector, with $\boldsymbol{S}^{(f)}$ being the vector of $(2f+1)\times(2f+1)$ matrices for spin f, and

$$A_0^{(2)} = \frac{1}{\sqrt{5}} \big(2\zeta_2^{(2)}\zeta_{-2}^{(2)} - 2\zeta_1^{(2)}\zeta_{-1}^{(2)} + \zeta_0^{(2)2} \big) \tag{4}$$

is the spin-singlet scalar for spin 2. The interaction coefficients in Eqs. (1) and (2) have the forms,

$$g_0^{(1)} = \frac{4\pi\hbar^2}{M_1} \frac{a_0^{(1)} + 2a_2^{(1)}}{3}, \tag{5a}$$

$$g_1^{(1)} = \frac{4\pi\hbar^2}{M_1} \frac{a_2^{(1)} - a_0^{(1)}}{3}, \tag{5b}$$

$$g_0^{(2)} = \frac{4\pi\hbar^2}{M_2} \frac{4a_2^{(2)} + 3a_4^{(2)}}{7}, \tag{5c}$$

$$g_1^{(2)} = \frac{4\pi\hbar^2}{M_2} \frac{a_4^{(2)} - a_2^{(2)}}{7}, \tag{5d}$$

$$g_2^{(2)} = \frac{4\pi\hbar^2}{M_2} \frac{7a_0^{(2)} - 10a_2^{(2)} + 3a_4^{(2)}}{7}, \tag{5e}$$

where $a_{\mathcal{F}}^{(f)}$ is the s-wave scattering length between spin-f atoms with colliding channel of total spin $\mathcal{F}$. We denote the spin vectors as $\boldsymbol{\zeta}^{(1)} = (\zeta_1^{(1)}, \zeta_0^{(1)}, \zeta_{-1}^{(1)})$ and $\boldsymbol{\zeta}^{(2)} = (\zeta_2^{(2)}, \zeta_1^{(2)}, \zeta_0^{(2)}, \zeta_{-1}^{(2)}, \zeta_{-2}^{(2)})$.

Before considering the mixture of spinor BECs, we summarize the ground-state phases for individual spin-1 and spin-2 BECs in a uniform system. The ground state of a spin-1 BEC depends on the sign of $g_1^{(1)}$. When $g_1^{(1)} < 0$, the ground state is the fully polarized ferromagnetic state,

$$\boldsymbol{\zeta}_F^{(1)} \equiv e^{i\chi} \hat{R}(1,0,0), \tag{6}$$

where χ is an arbitrary phase and $\hat{R}$ is an arbitrary SO(3) rotation in the spin space. When $g_1^{(1)} > 0$, the ground state is the polar state,

$$\boldsymbol{\zeta}_P^{(1)} \equiv e^{i\chi} \hat{R}(0,1,0). \tag{7}$$

The spin-2 BEC has more variety of ground states. When $g_1^{(2)} < 0$ and $g_2^{(2)} > 20 g_1^{(2)}$, the ground state is the ferromagnetic state,

$$\boldsymbol{\zeta}_F^{(2)} \equiv e^{i\chi} \hat{R}(1,0,0,0,0). \tag{8}$$

When $g_2^{(2)} < 0$ and $g_2^{(2)} < 20 g_1^{(2)}$, the ground state has continuous degeneracy: a linear combination of the uniaxial nematic state,

$$\boldsymbol{\zeta}_{\mathrm{UN}}^{(2)} \equiv e^{i\chi} \hat{R}(0,0,1,0,0), \tag{9}$$

and the biaxial nematic state,

$$\boldsymbol{\zeta}_{\mathrm{BN}}^{(2)} \equiv e^{i\chi} \hat{R}(1,0,0,0,1)/\sqrt{2}, \tag{10}$$

is the ground state. When $g_1^{(2)} > 0$ and $g_2^{(2)} > 0$, the ground state is the cyclic state,

$$\boldsymbol{\zeta}_C^{(2)} \equiv e^{i\chi} \hat{R}(1/2,0,i/\sqrt{2},0,1/2). \tag{11}$$

For later use, we define the state,

$$\boldsymbol{\zeta}_{F'}^{(2)} \equiv e^{i\chi} \hat{R}(0,1,0,0,0), \tag{12}$$

which is not the ground state but a stationary state of the Gross-Pitaevskii equation. The spherical harmonic representation of the spin state is convenient for visualizing the symmetry of the system [32],

$$S(\theta,\phi) = \sum_{m=-f}^{f} \zeta_m^{(f)} Y_f^m(\theta,\phi), \tag{13}$$

where Y_f^m is the spherical harmonics. The spherical harmonic representations of the above spin states are shown in Fig. 1.

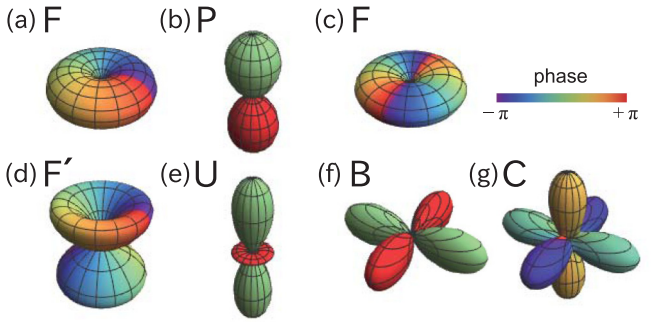

FIG. 1. Spherical harmonic representations $S(\theta,\phi)$ of the spin states. (a) Spin-1 ferromagnetic state $\boldsymbol{\zeta}_F^{(1)}$. (b) Spin-1 polar state $\boldsymbol{\zeta}_P^{(1)}$. (c) Spin-2 ferromagnetic state $\boldsymbol{\zeta}_F^{(2)}$. (d) Spin-2 state $\boldsymbol{\zeta}_{F'}^{(2)}$. (e) Spin-2 uniaxial nematic state $\boldsymbol{\zeta}_{\mathrm{UN}}^{(2)}$. (f) Spin-2 biaxial nematic state $\boldsymbol{\zeta}_{\mathrm{BN}}^{(2)}$. (g) Spin-2 cyclic state $\boldsymbol{\zeta}_C^{(2)}$. The labels F, P, F′, U, B, and C shown for each representation are used to identify the spin state in the phase diagram.

We consider a mixture of spin-1 and spin-2 BECs. The interaction energy between the spin-1 and spin-2 BECs is obtained to be (see appendix for derivation)

$$E_{12} = \int d\boldsymbol{r} \big[g_0^{(12)} + g_1^{(12)} \boldsymbol{F}^{(1)}(\boldsymbol{r}) \cdot \boldsymbol{F}^{(2)}(\boldsymbol{r}) + g_2^{(12)} P_1^{(12)}(\boldsymbol{r}) \big] \rho_1(\boldsymbol{r}) \rho_2(\boldsymbol{r}), \tag{14}$$

where $P_1^{(12)}$ is defined in Eq. (A7). The interaction coefficients in Eq. (14) are given by

$$g_0^{(12)} = \frac{2\pi\hbar^2}{M_{12}} \frac{2a_2^{(12)} + a_3^{(12)}}{3}, \tag{15a}$$

$$g_1^{(12)} = \frac{2\pi\hbar^2}{M_{12}} \frac{a_3^{(12)} - a_2^{(12)}}{3}, \tag{15b}$$

$$g_2^{(12)} = \frac{2\pi\hbar^2}{M_{12}} \frac{3a_1^{(12)} - 5a_2^{(12)} + 2a_3^{(12)}}{3}, \tag{15c}$$

where $M_{12} = (M_1^{-1} + M_2^{-1})^{-1}$ is the reduced mass and $a_{\mathcal{F}}^{(12)}$ is the s-wave scattering length between spin-1 and spin-2 atoms with colliding channel of total spin $\mathcal{F}$.

In the following analysis, we assume that the spin healing lengths are much larger than the size of the atomic cloud and we neglect the spatial variation of the spin states $\boldsymbol{\zeta}^{(f)}$. The kinetic and potential energy terms in E_1 and E_2 in Eqs. (1) and (2) then become independent of the spin states $\boldsymbol{\zeta}^{(f)}$. The spin-dependent part of the total energy $E = E_1 + E_2 + E_{12}$ thus reduces to

$$E_{\rm spin} = \frac{1}{2}\left(c_1^{(1)}\boldsymbol{F}^{(1)}\cdot\boldsymbol{F}^{(1)} + c_1^{(2)}\boldsymbol{F}^{(2)}\cdot\boldsymbol{F}^{(2)} + c_2^{(2)}\left|A_0^{(2)}\right|^2\right) + c_1^{(12)}\boldsymbol{F}^{(1)}\cdot\boldsymbol{F}^{(2)} + c_2^{(12)}P_1^{(12)}, \tag{16}$$

where

$$c_n^{(f)} = g_n^{(f)}\int \rho_f^2(\boldsymbol{r})d\boldsymbol{r},$$
$$c_n^{(12)} = g_n^{(12)}\int \rho_1(\boldsymbol{r})\rho_2(\boldsymbol{r})d\boldsymbol{r}, \tag{17}$$

with $n = 1,2$. In the rest of this paper, we normalize the interaction coefficients $c_n^{(f)}$ by $4\pi\hbar^2 a_B\int\rho_f^2 d\boldsymbol{r}/M_f$ and $c_n^{(12)}$ by $2\pi\hbar^2 a_B\int\rho_1\rho_2 d\boldsymbol{r}/M_{12}$, where a_B is the Bohr radius, and therefore these interaction coefficients are dimensionless.

Our purpose is to find the spin states $\boldsymbol{\zeta}^{(1)}$ and $\boldsymbol{\zeta}^{(2)}$ that minimize the energy $E_{\rm spin}$. We numerically obtain the ground state as follows. First we set complex random numbers to $\zeta_m^{(f)}$ and minimize the energy in a stochastic manner, that is, we try a small random change to the spin state $\zeta_m^{(f)} + \delta\zeta_m^{(f)}$ and adopt the change if the energy is lowered. After sufficiently many steps in this random walk in the spin space, we obtain a metastable state or the ground state. Repeating this procedure many times with different initial random states, we can exclude metastable states and determine the true ground state.

III. GROUND STATES OF A MIXTURE OF SPIN 1 AND SPIN 2

To see the effect of the interaction between the spin-1 and spin-2 BECs, we first consider the case without the intraspin interactions, $c_1^{(1)} = c_1^{(2)} = c_2^{(2)} = 0$. The spin-dependent energy then reduces to $E_{\rm spin} = c_1^{(12)}\boldsymbol{F}^{(1)}\cdot\boldsymbol{F}^{(2)} + c_2^{(12)}P_1^{(12)}$. Figure 2 shows the ground-state phase diagram with respect to $c_1^{(12)}$ and $c_2^{(12)}$, and Table I shows $E_{\rm spin}$ for each phase. When $c_1^{(12)}$ is sufficiently large and negative, the state in which the spin vectors $\boldsymbol{F}^{(1)}$ and $\boldsymbol{F}^{(2)}$ are fully polarized in the same direction is energetically favored, and the ground state is $\boldsymbol{\zeta}^{(1)} = \boldsymbol{\zeta}_F^{(1)}$ and $\boldsymbol{\zeta}^{(2)} = \boldsymbol{\zeta}_F^{(2)}$. We abbreviate this state as "FF$_+$," in which the first and second capital letters indicate the spin-1 and spin-2 states shown in Fig. 1, respectively, and the subscript + denotes that the two spin vectors are in the same direction. In a similar manner, when $c_1^{(12)}$ is large and positive, the ground state is the ferromagnetic state with $\boldsymbol{F}^{(1)}$ and $\boldsymbol{F}^{(2)}$ being in opposite directions. This phase is denoted as "FF$_-$," where the subscript $-$ represents that the two spin vectors are in the opposite directions. In general, we define the subscripts $\pm$ to indicate the sign of $\boldsymbol{F}^{(1)}\cdot\boldsymbol{F}^{(2)}$. As shown in Fig. 2, there are two regions between these ferromagnetic phases. When $c_2^{(12)} < 0$ and $c_2^{(12)}/5 < c_1^{(12)} < c_2^{(12)}/10$, the ground state is $\boldsymbol{\zeta}^{(1)} = \boldsymbol{\zeta}_P^{(1)}$ and $\boldsymbol{\zeta}^{(2)} = \boldsymbol{\zeta}_{\rm UN}^{(2)}$, which is denoted as "PU". When $c_2^{(12)} > 0$ and $0 < c_1^{(12)} < 3c_2^{(12)}/10$, the ground state is continuously degenerate: The linear combination of the "PF" (polar-ferromagnetic) and "PB" (polar-biaxial nematic) states is the ground state. We have numerically confirmed that the phase diagram in Fig. 2 is correct.

TABLE I. Spin-dependent energies $E_{\rm spin}$ for the phases in Fig. 2 with $c_1^{(1)} = c_1^{(2)} = c_2^{(2)} = 0$.

	$E_{\rm spin}$
FF$_+$	$2c_1^{(12)}$
FF$_-$	$-2c_1^{(12)} + 3c_2^{(12)}/5$
PU	$2\,c_2^{(12)}/5$
PF and PB	0

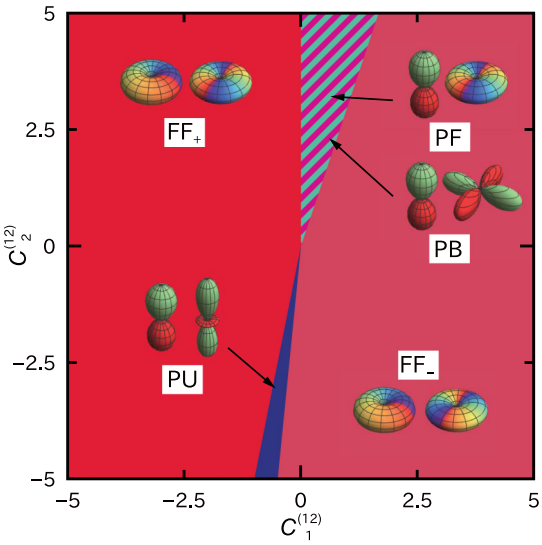

FIG. 2. Ground-state phase diagram with respect to the interspin interactions $c_1^{(12)}$ and $c_2^{(12)}$ without the intraspin interactions, $c_1^{(1)} = c_1^{(2)} = c_2^{(2)} = 0$. The spherical harmonic representations of the spin states are also shown, where the left- and right-hand figures indicate the spin-1 and spin-2 states, respectively. The letter pairs specify the spin-1 and spin-2 states, which are defined in Fig. 1, and the subscript $\pm$ indicates the sign of $\boldsymbol{F}^{(1)}\cdot\boldsymbol{F}^{(2)}$. In the striped region, the linear combination of the polar-ferromagnetic (PF) and polar-biaxial nematic (PB) states are continuously degenerate.

Next we consider the cases of nonzero intraspin interaction coefficients $c_1^{(1)}$, $c_1^{(2)}$, and $c_2^{(2)}$. Figure 3 shows the ground-state phase diagram for $c_1^{(1)} = -0.46$, $c_1^{(2)} = 1.1$, and $c_2^{(2)} = -0.05$, which correspond to the interaction coefficients of ^{87}Rb for $\rho_1 = \rho_2$ in Eq. (17). There is a remarkable number of phases with complicated structures. If the interspin interaction is absent, i.e., at the origin of the phase diagram, the ground state for spin 1 is the ferromagnetic state and that for spin 2 is the nematic state. Comparing Fig. 3 with Fig. 2, we find that the four phases in Fig. 2, FF$_+$, FF$_-$, PU, and PB, also appear in Fig. 3, where the continuous degeneracy in Fig. 2 is removed and the PF state disappears in Fig. 3. There are many

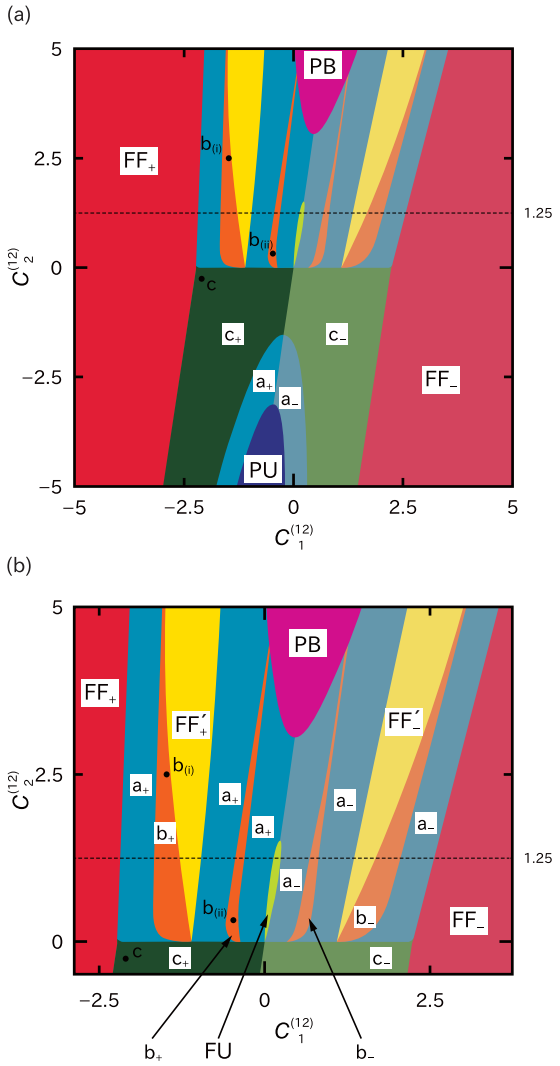

FIG. 3. Ground-state phase diagram for $c_1^{(1)} = -0.46$, $c_1^{(2)} = 1.1$, and $c_2^{(2)} = -0.05$. The ground state for $c_1^{(12)} = c_2^{(12)} = 0$ is the ferromagnetic state for spin 1 and the nematic state (linear combination of the U and B states) for spin 2. The region of many phases in (a) is magnified in (b). The upper-case letter pairs indicate the spin-1 and spin-2 states as defined in Fig. 1 and the lower-case letters indicate the intermediate states as defined in Table II. The subscripts ± denote the sign of $\boldsymbol{F}^{(1)} \cdot \boldsymbol{F}^{(2)}$. The physical quantities along the dotted line are shown in Fig. 4(a). The spin states at the black dots are shown in Fig. 4(b).

intermediate states, labeled by lower-case letters classified in Table II. In the regions of these intermediate states, either or both of the spin-1 and spin-2 states continuously change with respect to $c_1^{(12)}$ and $c_2^{(12)}$.

We now consider the phases along the dotted line in Fig. 3. When $c_1^{(12)}$ is large and negative, the ground state is the FF_+ state. When $c_1^{(12)}$ crosses the phase boundary between FF_+ and a_+, the lengths of the spin-1 and spin-2 vectors begin to decrease, as shown in Fig. 4(a). In this a_+ phase, the spin vectors $\boldsymbol{F}^{(1)}$ and $\boldsymbol{F}^{(2)}$ remain in the same direction. In contrast, in the b_+ phase, the directions of the spin vectors $\boldsymbol{F}^{(1)}$ and $\boldsymbol{F}^{(2)}$ become different. This can be regarded as axisymmetry

TABLE II. Classification of the intermediate states that change continuously in the phase diagram. "Nonzero" indicates that the value depends on $c_1^{(12)}$ and $c_2^{(12)}$. E indicates the trivial group. The subscript + or − is added to a–d to indicate the sign of $\boldsymbol{F}^{(1)} \cdot \boldsymbol{F}^{(2)}$.

	$\lvert\boldsymbol{F}^{(1)}\rvert$	$\lvert\boldsymbol{F}^{(2)}\rvert$	$A_0^{(2)}$	$\boldsymbol{F}^{(1)} \times \boldsymbol{F}^{(2)}$	Isotropy group
a	Nonzero	Nonzero	Nonzero	0	$\mathbb{Z}_2$
b	Nonzero	Nonzero	Nonzero	Nonzero	E
c	1	Nonzero	Nonzero	0	$\mathbb{Z}_4$
d	1	Nonzero	0	0	$\mathbb{Z}_3$
e	0	0	Nonzero	0	$\mathbb{Z}_2 \times \mathbb{Z}_2$

breaking of the magnetization, that is, if we fix the vector $\boldsymbol{F}^{(1)}$ to the z direction, the vector $\boldsymbol{F}^{(2)}$ has a component $F_\perp^{(2)}$ perpendicular to the z axis. Examples of such axisymmetry breaking states are shown in Fig. 4(b). Axisymmetry breaking has been found in a mixture of spin-1 and spin-1 BECs in the presence of an external magnetic field [24]. In the FF'_+ phase, the directions of the spin vectors $\boldsymbol{F}^{(1)}$ and $\boldsymbol{F}^{(2)}$ become the same again. In this phase, the spin-1 state returns to $\boldsymbol{\zeta}^{(1)} = \boldsymbol{\zeta}_F^{(1)}$ and the spin-2 state is $\boldsymbol{\zeta}^{(2)} = \boldsymbol{\zeta}_{F'}^{(2)}$, which does not depend on $c_1^{(12)}$ and $c_2^{(12)}$ within the phase, as seen from the plateau in Fig. 4(a). In the a_+, b_+, and a_+ phases, the spin states continuously change again; the spin vectors $\boldsymbol{F}^{(1)}$ and $\boldsymbol{F}^{(2)}$ are in the same direction in the a_+ phase, while they take different directions

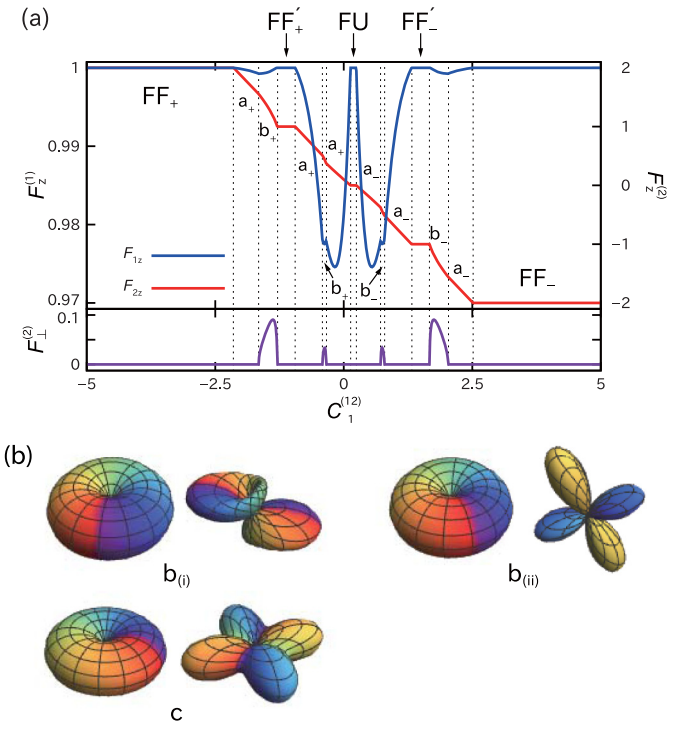

FIG. 4. (a) Dependence of $F_z^{(1)}$, $F_z^{(2)}$, and $F_\perp^{(2)}$ on $c_1^{(12)}$ along the dotted line in Fig. 3, where $F_\perp^{(f)} = [(F_x^{(f)})^2 + (F_y^{(f)})^2]^{1/2}$. Here, the spin-1 and spin-2 states are rotated so that $\boldsymbol{F}^{(1)}$ is in the z direction, and hence $F_\perp^{(1)}$ is always zero. (b) Spherical-harmonic representations of the spin states marked by the black dots in Fig. 3, where the left- and right-hand figures are the spin-1 and spin-2 states, respectively.

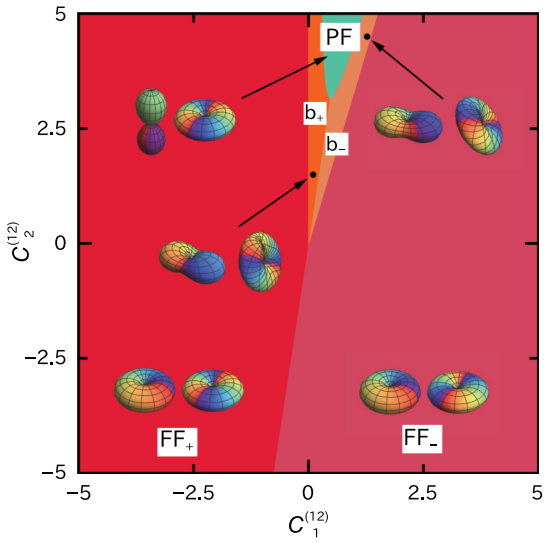

FIG. 5. Ground-state phase diagram for $c_1^{(1)} = -0.46$, $c_1^{(2)} = -1.1$, and $c_2^{(2)} = 1.5$. The ground state for $c_1^{(12)} = c_2^{(12)} = 0$ is the ferromagnetic state for both spin 1 and spin 2. The spherical harmonic representations of the spin states are also shown, where the left- and right-hand figures represent the spin-1 and spin-2 states, respectively.

in the b_+ phase. The FU phase is connected to the origin of the phase diagram; although a linear combination of the FU and FB states is the ground state at the origin, only the FU state occupies the finite region of the phase diagram. The phases on the right-hand side of the phase diagram, a_-, b_-, ... are similar to the corresponding phases a_+, b_+, ... where the spin vector $\boldsymbol{F}^{(1)}$ or $\boldsymbol{F}^{(2)}$ is flipped, i.e., the time-reversal transformation is applied to the spin-1 or spin-2 state. For example, in the FF'_- phase, when the spin-1 state is $\boldsymbol{\zeta}^{(1)} = (1,0,0)$, the spin-2 state is $\boldsymbol{\zeta}^{(2)} = (0,0,0,1,0)$, which is the time-reversal state of $\boldsymbol{\zeta}^{(2)} = (0,1,0,0,0)$ in the FF'_+ phase. For $c_2^{(12)} < 0$, the phase structures are simpler. In the $c_\pm$ phases, the spin-1 state is fixed to the ferromagnetic state, while the spin-2 state continuously changes with $\boldsymbol{F}^{(1)}$ and $\boldsymbol{F}^{(2)}$ being kept in the same direction. A typical c state is shown in Fig. 4(b).

In the experiment in Ref. [31], the values of the interspin scattering lengths of ^{87}Rb were measured, which correspond to $c_1^{(12)} \simeq 0.83$ and $c_2^{(12)} \simeq 4.8$ in the present case, if $\rho_1 = \rho_2$ in Eq. (17), i.e., an almost 1:1 mixture of spin-1 and spin-2 atoms. In the phase diagram in Fig. 3, these values correspond to the PB state, namely, the polar state for spin 1 and the biaxial nematic state for spin 2. The ground-state phase of the spin-1 ^{87}Rb BEC alone is the ferromagnetic state and that for spin 2 is the biaxial or uniaxial nematic state. Thus, the ground state of the 1:1 mixture of spin-1 and spin-2 ^{87}Rb BECs is different from those of the individual BECs due to the interspin interaction.

Figure 5 shows the ground-state phase diagram for $c_1^{(1)} = -0.46$, $c_1^{(2)} = -1.1$, and $c_2^{(2)} = 1.5$. If the interspin interaction is absent, the ground state is the ferromagnetic state both for spin 1 and spin 2 for these parameters. The phase diagram is much simpler than Fig. 3. Comparing Fig. 5 with Fig. 2, we find that the PB and PU states disappear in Fig. 5. Between the PF and $FF_\pm$ phases, there exists the region of the b state, in which the axisymmetry is broken. For the present parameters, the spin-2 state is almost the ferromagnetic state in the b phase. The angle between the two spin vectors changes from 0 to π across the region of the b state.

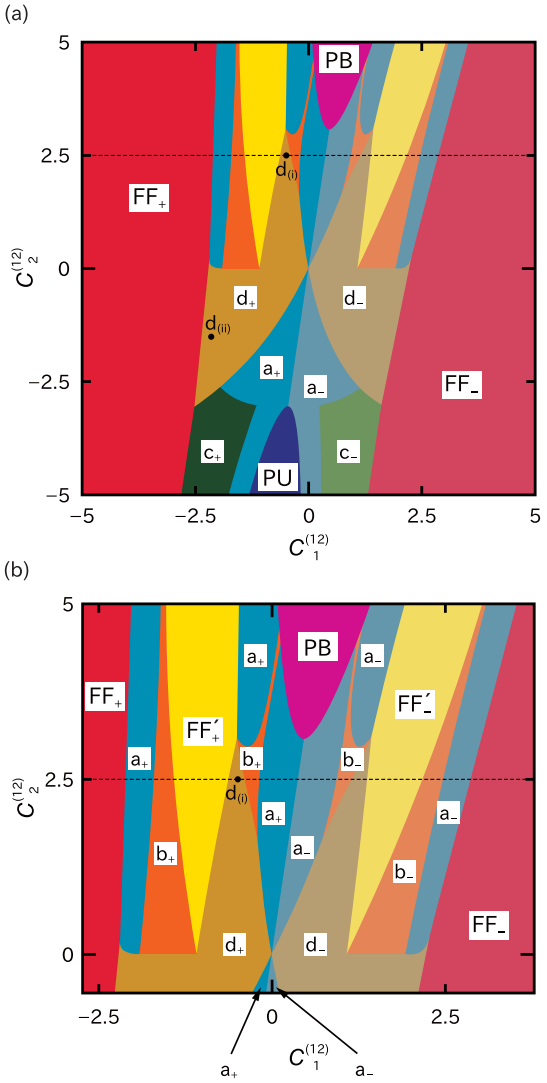

FIG. 6. Ground-state phase diagram for $c_1^{(1)} = -0.46$, $c_1^{(2)} = 1.1$, and $c_2^{(2)} = 1.5$. The ground state for $c_1^{(12)} = c_2^{(12)} = 0$ is the ferromagnetic state for spin 1 and the cyclic state for spin 2. The region of many phases in (a) is magnified in (b). The physical quantities along the dotted line are shown in Fig. 7(a). The spin states at the black dots are shown in Fig. 7(b).

Figure 6 shows the ground-state phase diagram for $c_1^{(1)} = -0.46$, $c_1^{(2)} = 1.1$, and $c_2^{(2)} = 1.5$. If the interspin interaction is absent, i.e., at the origin of the phase diagram, the ground state of the spin-1 BEC is the ferromagnetic state and that of the spin-2 BEC is the cyclic state for these parameters. The phase diagram is again very complicated. Let us examine the phases along the dotted line. As $c_1^{(12)}$ is increased from a large negative value, the ground state changes from the FF_+ state to the a_+, b_+, and FF'_+ states, which is similar to the case in Fig. 3. After that, a new phase appears, labeled by d_+. In this phase, the value of $|A_0^{(2)}|$ in the spin-2 state vanishes, as in the

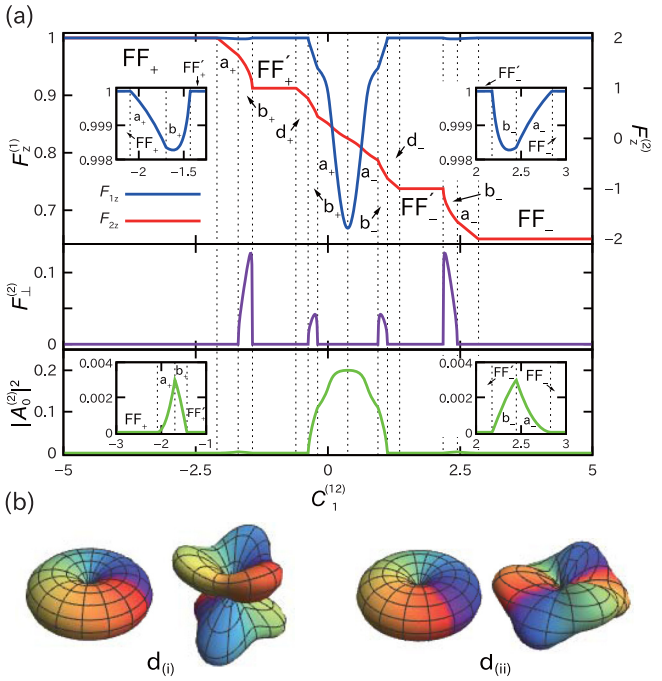

FIG. 7. (a) Dependence of $F_z^{(1)}$, $F_z^{(2)}$, $F_\perp^{(2)}$, and $|A_0^{(2)}|^2$ on $c_1^{(12)}$ along the dotted line in Fig. 6. Here, the spin-1 and spin-2 states are rotated so that $\boldsymbol{F}^{(1)}$ is in the z direction, and hence $F_\perp^{(1)}$ is always zero. The small changes in $F_z^{(1)}$ and $|A_0^{(2)}|^2$ are magnified in the insets. (b) Spherical-harmonic representations of the spin states marked by the black dots in Fig. 6, where the left- and right-hand figures are the spin-1 and spin-2 states, respectively.

cyclic state, whereas $|\boldsymbol{F}^{(2)}|$ is finite, as shown in Fig. 7(a). The spin-1 state is in the ferromagnetic state $\boldsymbol{\zeta}^{(1)} = \boldsymbol{\zeta}_F^{(1)}$. From the shape of the spherical harmonic representation in Fig. 7(b), we find that this state may be regarded as an intermediate state between the FC and FF′ states. The d$_\pm$ states also exist in the

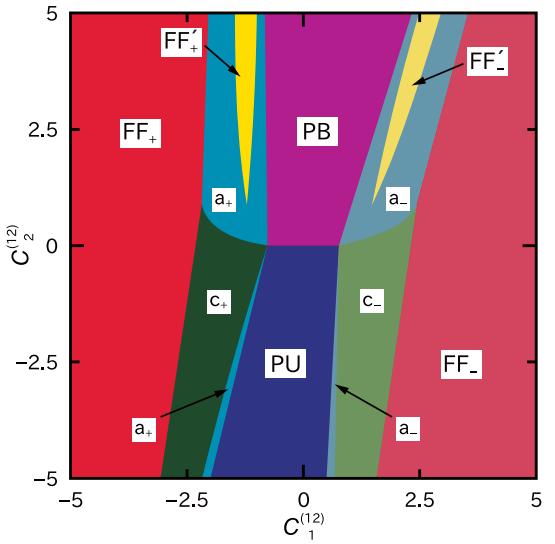

FIG. 8. Ground-state phase diagram for $c_1^{(1)} = 0.46$, $c_1^{(2)} = 1.1$, and $c_2^{(2)} = -1$. The ground state for $c_1^{(12)} = c_2^{(12)} = 0$ is the polar state for spin 1 and the nematic state for spin 2.

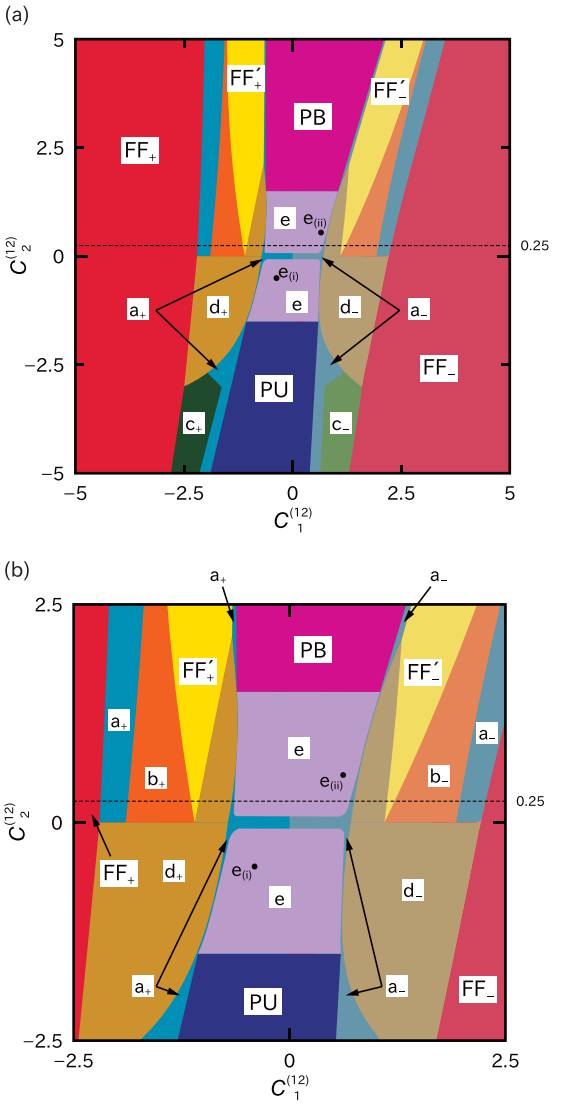

FIG. 9. Ground-state phase diagram for $c_1^{(1)} = 0.46$, $c_1^{(2)} = 1.1$, and $c_2^{(2)} = 1.5$. The ground state for $c_1^{(12)} = c_2^{(12)} = 0$ is the polar state for spin 1 and the cyclic state for spin 2. The region of many phases in (a) is magnified in (b). The physical quantities along the dotted line in (a) are shown in Fig. 10(a). The spin states at the black dots are shown in Fig. 10(b).

region $c_2^{(12)} < 0$. The structures of the a$_\pm$, b$_\pm$, and c$_\pm$ regions in Fig. 6 appear to be different from those in Fig. 3.

Figure 8 shows the ground-state phase diagram for $c_1^{(1)} = 0.46$, $c_1^{(2)} = 1.1$, and $c_2^{(2)} = -1$. If the interspin interaction is absent, the ground state of the spin-1 BEC is the polar state and that of the spin-2 BEC is the nematic state for these parameters. We find from Fig. 8 that the PB and PU phases extend and contact each other at $c_2^{(12)} = 0$. In this phase diagram there is no symmetry broken state, such as the b state.

Figure 9 shows the ground-state phase diagram for $c_1^{(1)} = 0.46$, $c_1^{(2)} = 1.1$, and $c_2^{(2)} = 1.5$. If the interspin interaction is absent, the ground state of the spin-1 BEC is the polar state and that of the spin-2 BEC is the cyclic state for these parameters. In this phase diagram, a new state appears, labeled e. The e state has no magnetization for both spin 1 and spin 2,

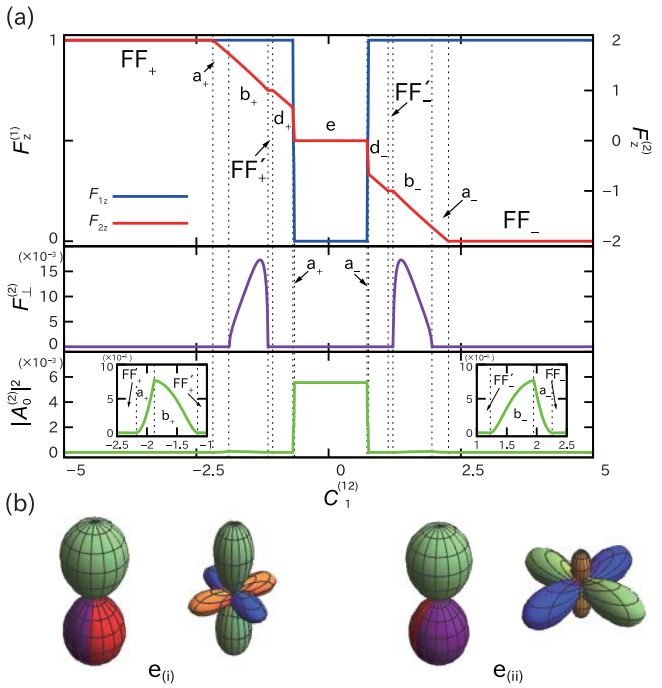

FIG. 10. (a) Dependence of $F_z^{(1)}$, $F_z^{(2)}$, $F_\perp^{(2)}$, and $|A_0^{(2)}|^2$ on $c_1^{(12)}$ along the dotted line in Fig. 9. Here, the spin-1 and spin-2 states are rotated so that $\boldsymbol{F}^{(1)}$ is in the z direction, and hence $F_\perp^{(1)}$ is always zero. The small changes in $|A_0^{(2)}|^2$ are magnified in the insets. (b) Spherical-harmonic representations of the spin states marked by the black dots in Fig. 6, where the left- and right-hand figures are the spin-1 and spin-2 states, respectively.

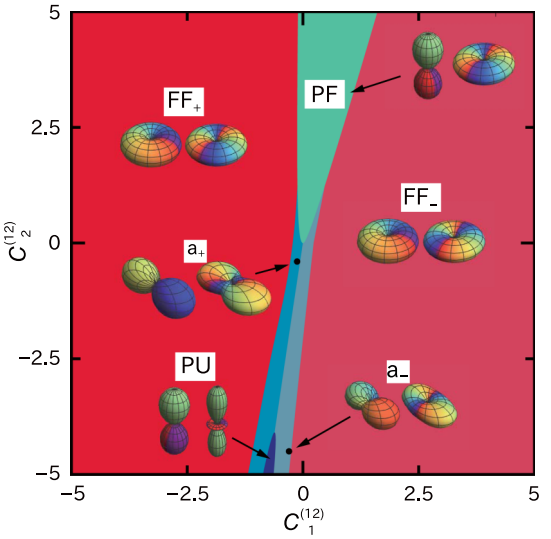

FIG. 11. Ground-state phase diagram for $c_1^{(1)} = 0.46$, $c_1^{(2)} = -0.0005$, and $c_2^{(2)} = 1$. The ground state for $c_1^{(12)} = c_2^{(12)} = 0$ is the polar state for spin 1 and the ferromagnetic state for spin 2. The spherical harmonic representations of the spin states are also shown, where the left- and right-hand figures represent the spin-1 and spin-2 states, respectively.

$\boldsymbol{F}^{(1)} = \boldsymbol{F}^{(2)} = 0$, as shown in Fig. 10(a). From the shapes of the spherical harmonic representation in Fig. 10(b), the e state is an intermediate state between the cyclic and nematic states. In the phase diagram, the regions of the e state are located at the heads of the PB and PU regions. For the parameters in Fig. 9, interestingly, the two regions of the e state are detached from each other near the origin, where the $a_\pm$ states fill in. Although in Fig. 10 the quantities $\boldsymbol{F}^{(1)}$, $\boldsymbol{F}^{(2)}$, and $A_0^{(2)}$ seem to jump at the boundary of the e region, they continuously change across the very narrow regions of the $a_\pm$ states. In all of the phase diagrams presented above, these quantities continuously change at the phase boundaries of the intermediate (a, b, c, d, and e) regions.

Figure 11 shows the ground-state phase diagram for $c_1^{(1)} = 0.46$, $c_1^{(2)} = -0.0005$, and $c_2^{(2)} = 1$. If the interspin interaction is absent, the ground state of the spin-1 BEC is the polar state and that of the spin-2 BEC is the ferromagnetic state for these parameters. We take the small value of $c_1^{(2)}$, because the PU region is far from the origin for a larger value of $c_1^{(2)}$. The $a_\pm$ states occupy the region near the origin instead of the PU state. Compared with Fig. 2, the degeneracy is removed and the PF state remains in the upper region of Fig. 11.

Finally, we mention the order-parameter manifold of the ground state. In the case of individual spin-1 and spin-2 BECs, the Hamiltonian is invariant with respect to changes in the global phase U(1), and the rotation in the spin space SO(3). The ground state therefore has continuous degeneracy, with a manifold represented by U(1) × SO(3). However, for example, the spin-1 ferromagnetic state in Fig. 1(a) is invariant with respect to rotation around the symmetry axis (with a global phase shift due to the spin-gauge symmetry). In other words, the isotropy group of the spin-1 ferromagnetic state is SO(2). The order-parameter manifold of the spin-1 ferromagnetic state is thus U(1) × SO(3) / SO(2) ≃ SO(3) [5]. The isotropy group of the spin-1 polar state is SO(2) $\times\mathbb{Z}_2$, since Fig. 1(b) is invariant with respect to rotation around the symmetry axis and upside-down rotation with global phase π.

In the case of the mixture of spin 1 and spin 2, the Hamiltonian is invariant with respect to changes in the global phase for each of the spin-1 and spin-2 states, in addition to the spin rotation of both spin-1 and spin-2 states, and then the symmetry group of the Hamiltonian is U(1) × U(1) × SO(3). For example, the isotropy group of the FF state is SO(2), and therefore the order-parameter manifold of the FF state is U(1) × SO(3). Similarly, the FF′ and FU states have this manifold. The isotropy groups of the intermediate states are summarized in Table II, whose symmetries are lower than those of individual spin states. For example, the symmetry-broken state b in Table II only has the trivial isotropy group (only the identity element).

IV. CONCLUSIONS

We have investigated the ground-state phase diagrams of a mixture of spin-1 and spin-2 BECs in the mean-field approximation. We obtained two types of ground states. One is a pair of known stationary states in spin-1 and spin-2 BECs, such as the FF and PB states. In the other type of ground state, either or both of the spin states continuously change with respect to the interaction coefficients. The latter type of ground state is classified in Table II.

For the various choices of the intraspin interaction coefficients, $c_1^{(1)}$, $c_1^{(2)}$, and $c_2^{(2)}$, we obtained the phase diagrams with respect to the interspin interaction coefficients, $c_1^{(12)}$ and $c_2^{(12)}$. These phase diagrams have remarkably rich structures. In all the phase diagrams, the FF_+ and FF_- phases occupy the regions of large negative and positive $c_1^{(12)}$, respectively. Also, the PF, or the PB and $\mathrm{FF}'_\pm$ phases are located in the $c_2^{(12)} > 0$ region, and the PU phase is located in the $c_2^{(12)} < 0$ region (except Fig. 5). Between these phases, there exist various intermediate phases with interesting phase structures. Among them, we found the axisymmetry broken phase (b in Table II), in which the spin-1 and spin-2 vectors are tilted from each other.

We have also determined the ground-state phase of a mixture of spin-1 and spin-2 ^{87}Rb BECs, using the measured interaction coefficients [31]. It has been known that the ground state of the spin-1 ^{87}Rb BEC alone is the ferromagnetic state and that of spin-2 BEC is a linear combination of the uniaxial and biaxial nematic states at zero magnetic field. By contrast, for an almost 1:1 mixture, the ground state is the polar state for spin 1 and the biaxial-nematic state for spin 2. The ground state of the spinor mixture of ^{87}Rb BECs is thus changed by the interaction between spin-1 and spin-2 BECs.

We have neglected the magnetic dipole-dipole interaction (DDI). This approximation is valid when the dimensionless ratio $\varepsilon_{\mathrm{dd}} = \mu_0\mu^2/(3g)$ is much smaller than unity, where μ_0 is the magnetic constant, μ is the magnetic moment of the spin-1 or -2 atom, and g is one of the coefficients in Eqs. (5) and (15). For $\varepsilon_{\mathrm{dd}} \sim 1$, we must consider the DDI energy given by

$$E_{\mathrm{ddi}} \propto \int d\boldsymbol{r}_1 d\boldsymbol{r}_2 \rho_1(\boldsymbol{r}_1)\rho_2(\boldsymbol{r}_2) \times \frac{\boldsymbol{F}^{(1)}\cdot\boldsymbol{F}^{(2)} - 3(\boldsymbol{F}^{(1)}\cdot\boldsymbol{e})(\boldsymbol{F}^{(2)}\cdot\boldsymbol{e})}{|\boldsymbol{r}_1-\boldsymbol{r}_2|^3}, \tag{18}$$

where $\boldsymbol{e} = (\boldsymbol{r}_1-\boldsymbol{r}_2)/|\boldsymbol{r}_1-\boldsymbol{r}_2|$. In Eq. (18), the spatial variation of the spin state is neglected on the same assumption in Eq. (16). If the density distributions ρ_1 and ρ_2 are isotropic, the integral in Eq. (18) vanishes and the DDI can be neglected even when $\varepsilon_{\mathrm{dd}} \sim 1$. On the other hand, if the density distributions are anisotropic, the anisotropic spin-dependent interaction emerges from Eq. (18). Moreover, if there exist some resonances, the dipolar effect may be enhanced [33].

The present study can be extended in various directions. For example, the magnetic field dependence (linear and quadratic) of the phase diagrams is the next planned extension of this work. Since the ground-state manifolds of the spinor mixture are different from those of single BECs, novel topological excitations will be possible. If phase separation occurs in the spinor mixture, we expect that the interface between domains will create interesting problems.

ACKNOWLEDGMENTS

This work was supported by JSPS KAKENHI Grants No. JP17K05595, No. JP17K05596, No. JP25103007, No. JP16K05505, and No. JP15K05233. Y.E. acknowledges support from Leading Initiative for Excellent Young Researchers (LEADER).

APPENDIX A: DERIVATION OF INTERACTION ENERGY BETWEEN SPIN-1 AND SPIN-2 ATOMS

The spin state of colliding spin-1 and spin-2 atoms can be represented by the bases as

$$|\mathcal{F},M\rangle = \sum_{mm'} C^{\mathcal{F}M}_{mm'}|1,m\rangle|2,m'\rangle, \tag{A1}$$

where $C^{\mathcal{F}M}_{mm'}$ is the Clebsch-Gordan coefficient, $\mathcal{F} = 1, 2$, and 3 are total spin, and $\mathcal{M} = -\mathcal{F}, -\mathcal{F}+1, \ldots, \mathcal{F}$. The projection operator for the colliding channel of total spin $\mathcal{F}$ is defined by

$$\hat{P}_{\mathcal{F}} = \sum_{\mathcal{M}=-\mathcal{F}}^{\mathcal{F}} |\mathcal{F},M\rangle\langle\mathcal{F},M|, \tag{A2}$$

which is rotation invariant. In the present Hilbert space, the identity operator $\hat{I}$ is given by

$$\hat{P}_1 + \hat{P}_2 + \hat{P}_3 = \hat{I}. \tag{A3}$$

We define the spin operators acting on the spin-1 and spin-2 states as $\hat{\boldsymbol{f}}_1$ and $\hat{\boldsymbol{f}}_2$, respectively. We find

$$\hat{\boldsymbol{f}}_1\cdot\hat{\boldsymbol{f}}_2 = \frac{1}{2}\left(\hat{\boldsymbol{f}}_1+\hat{\boldsymbol{f}}_2\right)^2 - \frac{1}{2}\sum_{f=1,2} f(f+1)\hat{I} = \frac{1}{2}\sum_{\mathcal{F}=1,2,3}\mathcal{F}(\mathcal{F}+1)\hat{P}_{\mathcal{F}} - 4\hat{I}. \tag{A4}$$

Since the Hamiltonian must be rotation invariant, the two-body interaction Hamiltonian between spin-1 and spin-2 atoms is written as

$$\hat{H}_{12} = \frac{2\pi\hbar^2}{M_{12}}\sum_{\mathcal{F}=1,2,3} a_{\mathcal{F}}\hat{P}_{\mathcal{F}}\delta(\boldsymbol{r}_1-\boldsymbol{r}_2), \tag{A5}$$

where $M_{12} = (M_1^{-1}+M_2^{-1})^{-1}$ is the reduced mass. Using Eqs. (A3) and (A4), the interaction Hamiltonian can be rewritten as

$$\hat{H}_{12} = \left(g_0^{(12)}\hat{I} + g_1^{(12)}\hat{\boldsymbol{f}}_1\cdot\hat{\boldsymbol{f}}_2 + g_2^{(12)}\hat{P}_1\right)\delta(\boldsymbol{r}_1-\boldsymbol{r}_2), \tag{A6}$$

where $g_0^{(12)}$, $g_1^{(12)}$, and $g_2^{(12)}$ are defined in Eq. (15). The mean-field energy is thus given by Eq. (14), where $P_1^{(12)} = |A_{1,1}|^2 + |A_{1,0}|^2 + |A_{1,-1}|^2$ with

$$A_{1,1} = \frac{1}{\sqrt{10}}\zeta_1^{(1)}\zeta_0^{(2)} - \sqrt{\frac{3}{10}}\zeta_0^{(1)}\zeta_1^{(2)} + \sqrt{\frac{3}{5}}\zeta_{-1}^{(1)}\zeta_2^{(2)}, \tag{A7a}$$

$$A_{1,0} = \sqrt{\frac{3}{10}}\zeta_1^{(1)}\zeta_{-1}^{(2)} - \sqrt{\frac{2}{5}}\zeta_0^{(1)}\zeta_0^{(2)} + \sqrt{\frac{3}{10}}\zeta_{-1}^{(1)}\zeta_1^{(2)}, \tag{A7b}$$

$$A_{1,-1} = \sqrt{\frac{3}{5}}\zeta_1^{(1)}\zeta_{-2}^{(2)} - \sqrt{\frac{3}{10}}\zeta_0^{(1)}\zeta_{-1}^{(2)} + \frac{1}{\sqrt{10}}\zeta_{-1}^{(1)}\zeta_0^{(2)}. \tag{A7c}$$

APPENDIX B: LINEAR STABILITY ANALYSIS AND PHASE BOUNDARIES

We perform a linear stability analysis of a stationary state to obtain the phase boundaries analytically. The total energy is

given by

$$E = \frac{c_0^{(1)}}{2}\left(\sum_{m=-1}^{1}\left|\zeta_m^{(1)}\right|^2\right)^2 + \frac{c_0^{(2)}}{2}\left(\sum_{m=-2}^{2}\left|\zeta_m^{(2)}\right|^2\right)^2 + \frac{1}{2}\left(c_1^{(1)}\boldsymbol{F}^{(1)}\cdot\boldsymbol{F}^{(1)} + c_1^{(2)}\boldsymbol{F}^{(2)}\cdot\boldsymbol{F}^{(2)} + c_2^{(2)}\left|A_0^{(2)}\right|^2\right) + c_1^{(12)}\boldsymbol{F}^{(1)}\cdot\boldsymbol{F}^{(2)} + c_2^{(12)}P_1^{(12)}. \tag{B1}$$

Using this energy, the Gross-Pitaevskii (GP) equation is written as

$$i\hbar\frac{\partial\zeta_m^{(f)}}{\partial t} = \frac{\partial E}{\partial\zeta_m^{(f)*}}. \tag{B2}$$

All of the ground states in the phase diagrams are stationary solutions of the GP equation. We write a stationary solution as

$$\zeta_m^{(f)}(t) = e^{-i\mu_f t/\hbar}Z_m^{(f)}, \tag{B3}$$

where μ_f is the chemical potential for spin f. We consider a small deviation from the stationary solution as

$$\zeta_m^{(f)}(t) = e^{-i\mu_f t/\hbar}\left(Z_m^{(f)} + u_m^{(f)}e^{-i\omega t} + v_m^{(f)*}e^{i\omega^* t}\right). \tag{B4}$$

Substituting this into Eq. (B2) and taking the first-order terms of $u_m^{(f)}$ and $v_m^{(f)}$, we obtain an 8×8 eigenvalue equation with respect to ω. If one or more eigenvalues are negative or complex, the stationary state $Z_m^{(f)}$ is not the ground state.

For example, we take the stationary state $Z_m^{(f)}$ as the ferromagnetic state $\boldsymbol{\zeta}^{(1)} = (1,0,0)$ and $\boldsymbol{\zeta}^{(2)} = (1,0,0,0,0)$, which corresponds to the FF_+ state in the phase diagrams. Diagonalizing the eigenvalue equation, we obtain

$$\omega = -3c_1^{(12)}, \tag{B5a}$$

$$\omega = -6c_1^{(2)} - 3c_1^{(12)} + \frac{3}{10}c_2^{(12)}, \tag{B5b}$$

$$\omega = -8c_1^{(2)} + \frac{2}{5}c_2^{(2)} - 4c_1^{(12)} + \frac{3}{5}c_2^{(12)}, \tag{B5c}$$

$$\omega = -c_1^{(1)} - 2c_1^{(2)} - 3c_1^{(12)} + \frac{7}{20}c_2^{(12)} \pm \left[A^2 - \frac{1}{2}Ac_2^{(12)} + \left(\frac{7}{20}c_2^{(12)}\right)^2\right]^{1/2}, \tag{B5d}$$

and $\omega = 0$, where $A = c_1^{(1)} - 2c_1^{(2)} + c_1^{(12)}$. In the case of Fig. 2, for example, the condition $\omega > 0$ for Eqs. (B5a) and (B5c) gives $c_1^{(12)} < 0$ and $c_2^{(12)} > 10c_2^{(12)}$, which agree with the phase boundary of the FF_+ phase in Fig. 2. On the other hand, for the phase diagram in Fig. 3, the phase boundary of the FF_+ phase is determined by Eqs. (B5c) and (B5d) for $c_2^{(12)} < 0$ and $c_2^{(12)} > 0$, respectively.

Taking the stationary state $Z_m^{(f)}$ as $\boldsymbol{\zeta}^{(1)} = (1,0,0)$ and $\boldsymbol{\zeta}^{(2)} = (0,0,0,0,1)$, i.e., the FF_- state, we obtain

$$\omega = -6c_1^{(2)} + 3c_1^{(12)} - \frac{3}{5}c_2^{(12)}, \tag{B6a}$$

$$\omega = -8c_1^{(2)} + \frac{2}{5}c_2^{(2)} + 4c_1^{(12)} - \frac{3}{5}c_2^{(12)}, \tag{B6b}$$

$$\omega = \pm\left(-c_1^{(1)} + 2c_1^{(2)} + c_1^{(12)} - \frac{1}{20}c_2^{(12)}\right) + \left[B^2 - \frac{11}{10}Bc_2^{(12)} + \frac{97}{400}c_2^{(12)2}\right]^{1/2}, \tag{B6c}$$

$$\omega = \left|c_1^{(12)} - \frac{3}{10}c_2^{(12)}\right|, \tag{B6d}$$

and $\omega = 0$, where $B = c_1^{(1)} + 2c_1^{(2)} - 3c_1^{(12)}$. For example, for the phase diagram in Fig. 3, the phase boundary of the FF_- phase is determined by Eqs. (B6b) and (B6c) for $c_2^{(12)} < 0$ and $c_2^{(12)} > 0$, respectively.

[1] D. Vollhardt and P. Wölfle, *The Superfluid Phases of Helium 3* (Taylor and Francis, London, 1990).
[2] M. R. Norman, Science **332**, 196 (2011).
[3] M. Hoffberg, A. E. Glassgold, R. W. Richardson, and M. Ruderman, Phys. Rev. Lett. **24**, 775 (1970).
[4] R. Tamakagaki, Prog. Theor. Phys. **44**, 905 (1970).
[5] T.-L. Ho, Phys. Rev. Lett. **81**, 742 (1998).
[6] T. Ohmi and K. Machida, J. Phys. Soc. Jpn. **67**, 1822 (1998).
[7] D. M. Stamper-Kurn, M. R. Andrews, A. P. Chikkatur, S. Inouye, H.-J. Miesner, J. Stenger, and W. Ketterle, Phys. Rev. Lett. **80**, 2027 (1998).
[8] J. Stenger, S. Inouye, D. M. Stamper-Kurn, H.-J. Miesner, A. P. Chikkatur, and W. Ketterle, Nature (London) **396**, 345 (1998).
[9] H. Schmaljohann, M. Erhard, J. Kronjäger, M. Kottke, S. van Staa, L. Cacciapuoti, J. J. Arlt, K. Bongs, and K. Sengstock, Phys. Rev. Lett. **92**, 040402 (2004).
[10] T. Kuwamoto, K. Araki, T. Eno, and T. Hirano, Phys. Rev. A **69**, 063604 (2004).
[11] B. Naylor, M. Brewczyk, M. Gajda, O. Gorceix, E. Maréchal, L. Vernac, and B. Laburthe-Tolra, Phys. Rev. Lett. **117**, 185302 (2016).
[12] M. W. Ray, E. Ruokokoski, S. Kandel, M. Möttönen, and D. S. Hall, Nature (London) **505**, 657 (2014).
[13] L. S. Leslie, A. Hansen, K. C. Wright, B. M. Deutsch, and N. P. Bigelow, Phys. Rev. Lett. **103**, 250401 (2009).
[14] S. W. Seo, S. Kang, W. J. Kwon, and Y.-I. Shin, Phys. Rev. Lett. **115**, 015301 (2015).
[15] D. S. Hall, M. W. Ray, K. Tiurev, E. Ruokokoski, A. H. Gheorghe, and M. Möttönen, Nat. Phys. **12**, 478 (2016).
[16] M. Koashi and M. Ueda, Phys. Rev. Lett. **84**, 1066 (2000).
[17] C. V. Ciobanu, S.-K. Yip, and T.-L. Ho, Phys. Rev. A **61**, 033607 (2000).
[18] M. Kobayashi, Y. Kawaguchi, M. Nitta, and M. Ueda, Phys. Rev. Lett. **103**, 115301 (2009).
[19] M. Luo, Z. Li, and C. Bao, Phys. Rev. A **75**, 043609 (2007).
[20] Z. F. Xu, Y. Zhang, and L. You, Phys. Rev. A **79**, 023613 (2009).
[21] Y. Shi, Phys. Rev. A **82**, 023603 (2010).
[22] Z. F. Xu, J. Zhang, Y. Zhang, and L. You, Phys. Rev. A **81**, 033603 (2010).
[23] J. Zhang, Z. F. Xu, L. You, and Y. Zhang, Phys. Rev. A **82**, 013625 (2010).

[24] Z. F. Xu, J. W. Mei, R. Lü, and L. You, Phys. Rev. A **82**, 053626 (2010).
[25] Y. Shi and L. Ge, Phys. Rev. A **83**, 013616 (2011).
[26] J. Zhang, T. Li, and Y. Zhang, Phys. Rev. A **83**, 023614 (2011).
[27] Z. F. Xu, R. Lü, and L. You, Phys. Rev. A **84**, 063634 (2011).
[28] Z. F. Xu, D. J. Wang, and L. You, Phys. Rev. A **86**, 013632 (2012).
[29] J. Zhang, X. Hou, B. Chen, and Y. Zhang, Phys. Rev. A **91**, 013628 (2015).
[30] X. Li, B. Zhu, X. He, F. Wang, M. Guo, Z.-F. Xu, S. Zhang, and D. Wang, Phys. Rev. Lett. **114**, 255301 (2015).
[31] Y. Eto, H. Shibayama, H. Saito, and T. Hirano, Phys. Rev. A **97**, 021602 (2018).
[32] Y. Kawaguchi and M. Ueda, Phys. Rep. **520**, 253 (2012).
[33] K. Gawryluk, M. Brewczyk, K. Bongs, and M. Gajda, Phys. Rev. Lett. **99**, 130401 (2007).